Classification of Shell-Shaped Targets Using RCS and Fuzzy Classifier

Seung-Jae Lee, Seong-Jae Jeong, Byung-Soo Kang, Hyun Kim, Sang-Mi Chon, Hyung-Gi Na, and Kyung-Tae Kim

***Abstract*—In this paper, a procedure to design a fuzzy classifier to classify shell-shaped targets is proposed. The proposed procedure utilizes the radar cross section (RCS) of a shell-shaped target considering the relative orientation angle and polarization dependences in various flight scenarios based on real situations. In addition, particle swarm optimization (PSO) is applied to the fuzzy classifier to maximize its classification capability. Numerical results using three different shell-shaped targets are presented to assess the effectiveness of the proposed method.**

***Index Terms*—Firefinder, fuzzy classifier, radar cross section (RCS), target classification.**

I. Introduction

FIREFINDER is a battlefield radar which rapidly and automatically locates enemy rocket launchers, artillery, and mortars [1]. The Firefinder radar can detect and track shell launching from enemy bases and acquire the trajectory of the shell. Then, the location of the weapon can be identified by processing trajectory data [2]–[7]. While the Firefinder locates the weapon of the enemy, additional information such as the type of shell can provide much assistance to friendly forces. Using information about the type of the shell, friendly forces can determine strategy and tactics as well as intercept the shell properly to protect bases occupied by friendly forces. Thus, accurate classification of the shell is an essential factor in real situations.

Radar can use many features such as radar cross section (RCS), high-resolution range profiles (HRRPs), inverse synthetic aperture radar (ISAR) images, and micro-Doppler signatures [8], [9]. Among them, RCSs are exploited to classify shell targets in this study. It should be noted that the Firefinder makes use of a very narrow frequency band with a very high pulse repetition frequency (PRF) because it is a time-critical targeting aid. In other words, the Firefinder should detect and track shell targets very rapidly such that overall detection, tracking, and classification times become as small as possible. Meanwhile, HRRPs, ISAR images, and micro-Doppler signatures require not only a wide frequency bandwidth but also a significant amount of processing time, which is inappropriate for classifying shell targets using the Firefinder.

Of course, different features such as drag coefficients and muzzle velocity of the shells, elevation angle of fire, and RCS can be combined to use as features to enhance classification capability. However, in this paper, only the RCS of shells is considered as a classification feature. Although RCS is a good candidate for classifying the shell, classification using RCS still has crucial disadvantages. Because RCS is sensitive to the relative aspect angle, classification accuracy using RCS is usually unreliable.

Some approaches to overcome this problem have been proposed [10], [11]. In [10], the maximum scatter difference (MSD) algorithm was used to extract the additional feature from RCS. The basic concept of the MSD algorithm is to seek the most discriminating features for the optimal projection direction so that maximum between-class scatter distance and minimum within-class scatter distance can be achieved in the projection direction. In the classification of ship targets, the classification accuracy using MSD was higher than that using other methods such as Fisher linear discriminant analysis (FLDA), *k*-nearest neighbor (KNN), and the classification and regression tree (CART) [10]. However, although MSD can improve the classification accuracy, additional signal processing steps and time to extract the features is needed. In other words, this method is inappropriate for classifying time-critical shell targets. In [11], a serial and decentralized fusion approach using RCS was proposed for the classification of re-entry vehicles (RVs) and spent tanks. Many local decisions based on statistics were used to make a global decision according to a specific fusion rule. However, this method is limited to discrimination of RV and spent tank because RCS of RV and spent tank are almost uncorrelated, leading to a relatively easy classification task.

In order to classify shell targets within a very short period of time, we selected a fuzzy classifier, which consists of membership functions (MFs) from targets to be classified. The MF relates the input value (i.e., the RCS value in this paper) to the probability that the input belongs to each specific target class. Therefore, the true target class can be automatically determined by the class of MF having the maximum probability. The neuro-fuzzy paradigm in this study can be easily extended to multi-input situations once multi-MFs corresponding to multi-input are determined. In classifying shell targets, the Firefinder radar may use multiple features (e.g., multi-input), including drag coefficients, the muzzle velocity of shells, and the elevation angle of fire, in addition to RCS, to improve classification performance. This implies that the fuzzy classifier is very useful

Manuscript received June 01, 2015; revised October 21, 2015; accepted January 18, 2016. Date of publication February 05, 2016; date of current version April 05, 2016. This work was supported by LIG Nex1 Co., Ltd.

S.-J. Lee, S.-J. Jeong, B.-S. Kang, and K.-T. Kim are with the Department of Electrical Engineering, Pohang University of Science and Technology, Pohang 790-784, Korea (e-mail: jelline15@postech.ac.kr; sungjaejung7@gmail.com; shipshong@postech.ac.kr; kkt@postech.ac.kr).

H. Kim, S.-M. Chon, and H.-G. Na are with LIG Nex1 Co., Ltd, Yongin 446-798, Korea (e-mail: hyun.kim@lignex1.com; chonsangmi369a@lignex1.com; hyunggi.na@lignex1.com).

Color versions of one or more of the figures in this paper are available online at http://ieeexplore.ieee.org.

Digital Object Identifier 10.1109/TAP.2016.2526059

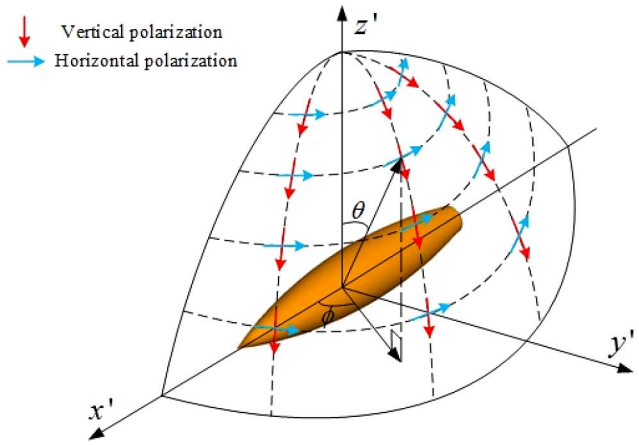

Fig. 1. 2-D grid with uniform angular intervals based on the spherical coordinates system.

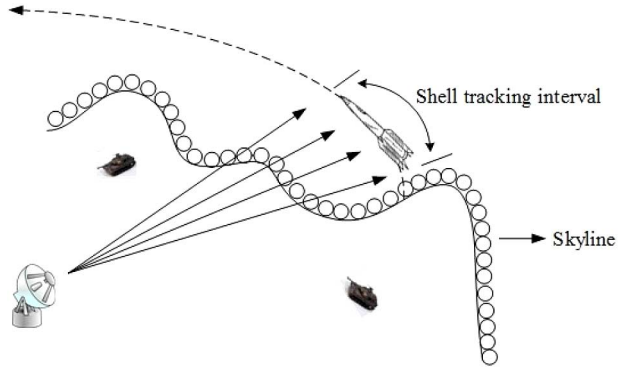

Fig. 2. Operational concept of the Firefinder.

for the Firefinder radars that require both a time-critical mission and multi-input situations.

Although the fuzzy classifier is computationally simple and efficient, the MFs should be chosen carefully to maximize the classification performance. There are a number of different MFs such as Gaussian, trapezoidal, and triangle MF. In particular, each MF is specified by a few parameters that determine the detailed shape and location of each MF. In this paper, we propose a method for optimizing MF parameters in order to obtain a high classification accuracy of shell targets in the Firefinder radar.

To optimize the parameters of MFs, we first set the various flight scenarios of the shell based on real situations. Next, the initial locations of MFs corresponding to each shell are determined using the RCS values obtained from the flight scenarios. Then, the parameters of MFs are optimized with the particle swarm optimization (PSO) algorithm to obtain the best performance of the fuzzy classifier.

This paper is organized as follows. The construction of the training database is explained in Section II. Section III presents the basic fuzzy set theory and MFs, as well as the optimization theory, used in this paper. Numerical results using computed RCS values via commercial software are presented in Section IV, and Section V concludes this paper.

II. Construction of Training Database

A. Construction of RCS Database

To construct the training database, we first create a two-dimensional (2-D) grid with uniform angular intervals along azimuth ϕ and elevation θ based on the spherical coordinates system (Fig. 1).

Then, RCS values reflected from a shell at each specific azimuth and elevation angle (i.e., a point in the 2-D grid) were computed using an electromagnetic numerical method and were stored in the RCS database. In addition, to construct the training database, RCSs using two different polarization channels such as vertical-to-vertical (VV) and horizontal-to-horizontal (HH) were obtained. Provided that the number of shells to be classified is L, and the number of samples along the azimuth and elevation are M and N, respectively, then the size of the RCS database yields $2 \times L \times M \times N$.

In this study, the method of moments (MoM) was used to compute the RCS because its RCS prediction accuracy is very high at the expense of its increased computation time [12].

B. Construction of Training Database Based on the Flight Scenario

The constructed entire RCS database can be directly used to design the fuzzy classifier to classify shells. However, the Firefinder radar usually collects RCS values of shells within a very limited measurement time.

The Firefinder usually searches and detects the shell along the skyline (Fig. 2). If the shell is detected above the skyline, the Firefinder starts to collect the RCS of the shell and remains in tracking mode for a few seconds. This in turn implies that the angular regions of collected RCS values occupy a very small portion of the constructed entire RCS database of shells.

A typical trace of shells during the measurement of the Firefinder is illustrated in a 2-D uniform angular domain, as shown in Fig. 3. The narrow distribution of the relative orientation angles means that we need not use the entire RCS database to construct the training database. Instead, we use only the RCS values related to small angular regions (i.e., relative orientation angles in a typical flight scenario). It is noted that actual relative orientation angles of a maneuvering shell have nonuniform intervals in the azimuth and elevation angular domain. This is because the Firefinder radar tracks shells with a uniform pulse repetition interval (PRI) in the time domain, leading to a nonuniform PRI in the angle domain. Thus, unknown RCS values with nonuniform sampling grids should be predicted via interpolation from the constructed RCS database with a uniform sampling grid, as shown in Fig. 3.

In order to construct the training database, three different typical flight scenarios corresponding to three different shell types are generated. The three scenarios have different initial velocities, elevation angles of fire, and locations of fire, which will be shown later. Next, the constructed uniform RCS database is interpolated to provide RCS values corresponding to the orientation angles in each flight scenario. Then, the interpolated RCS values of each flight scenario are averaged to produce a single mean RCS value, which will be used as training data.

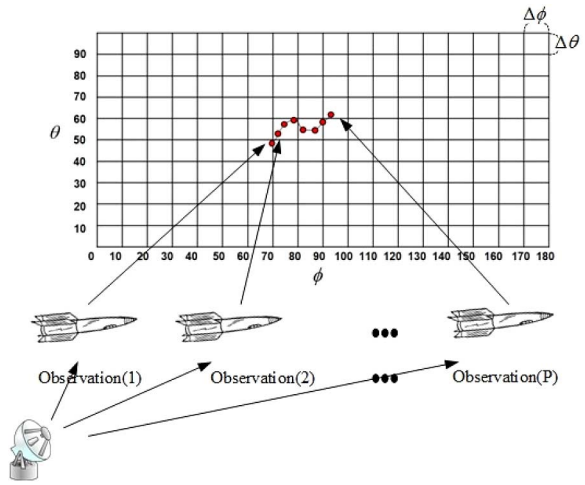

Fig. 3. Distribution of relative orientation angles in real situations.

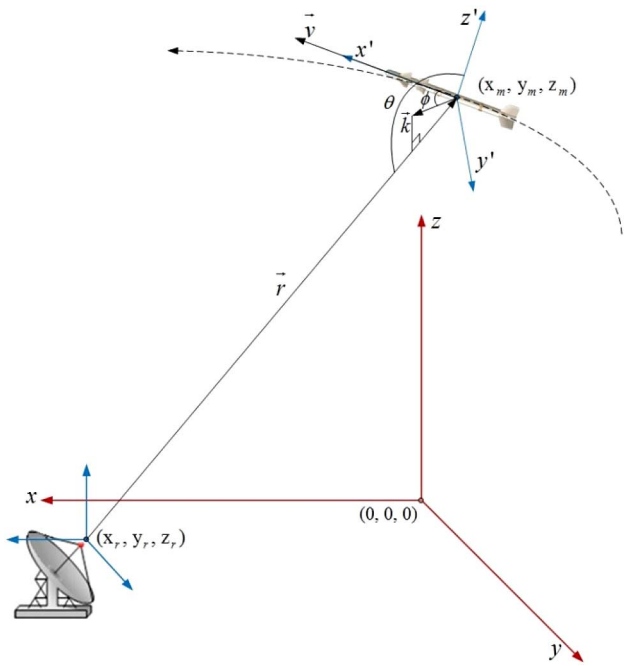

Fig. 4. Relative orientation angles of shell.

C. Consideration of Orientation Angle Dependence

Once Firefinder begins to track a flying shell, the RCS value reflected from the shell is varied depending on the relative orientation angles of the shell. When the shell flies in the direction of a vector $\overrightarrow{v}$, the local coordinate (x', y', z') of the shell is formed at every PRI, as shown in Fig. 4.

In Fig. 4, x' is assumed to be coincident with the direction of $\overrightarrow{v}$, $\overrightarrow{r}$ is the radar's line of sight (RLOS) vector, and $\overrightarrow{k}$ is the projection of the vector $\overrightarrow{r}$ onto the $x'-y'$ plane. Then, the elevation angle θ is defined as the angle between z' and $\overrightarrow{r}$. Furthermore, the azimuth angle ϕ is the angle between x' and $\overrightarrow{k}$. Let x', y', and z' be the unit vectors along x', y', and z', respectively. Then, θ and ϕ (i.e., the orientation angle) of the shell can be found as follows:

$$\theta = \cos^{-1}\left(\widehat{z}' \cdot (-\widehat{r})\right)$$
$$\phi = \cos^{-1}\left(\frac{x' \cdot \overrightarrow{k}}{\left|\overrightarrow{k}\right|}\right) \tag{1}$$

where $\overrightarrow{k} = -\overrightarrow{r} - \left(\widehat{z}' \cdot (-\overrightarrow{r})\right)\widehat{z}'$, $\widehat{r}$ is $\widehat{r} = \overrightarrow{r}/|\overrightarrow{r}|$, and $\cdot$ denotes the inner product. It should be noticed that x', y', z', θ, and ϕ in Fig. 4 are the same as those in Fig. 1. This means that we already have the RCS values in a uniform orientation angle grid in the RCS database. Thus, the RCS value at θ and ϕ in (1) can be obtained by interpolating from the given RCS database.

If Firefinder can estimate the exact roll angle of a flying shell in an actual situation, exact RCS of the shell can be obtained from a combination of elevation angle and azimuth angle and roll angle. However, the roll angle of the shell is not used in this study, because the Firefinder cannot measure the roll angle of a shell in general. Instead, it is assumed that the roll angle of the shell has a random value in the range of $0^\circ - 360^\circ$ with uniform probability density function (pdf), because the shell rotates about its axis at high speed.

D. Consideration of Polarization Dependence

Although the orientation-angle dependence of RCS was considered, the polarization of the shell also affects the RCS of the shell. Let $\widehat{s}_v$ and $\widehat{s}_h$ denote the unit vectors corresponding to the vertical and horizontal polarizations, respectively. As mentioned in Section II-A, the RCS database consists of RCS_{VV} and RCS_{HH}, which are the RCS values associated with VV and HH polarization, respectively. In an actual situation, if the copolarization direction of an antenna $\widehat{i}$ is identical to $\widehat{s}_v$ or $\widehat{s}_h$, the RCS of the shell can be obtained simply from either RCS_{VV} or RCS_{HH}. However, because the moving direction $\overrightarrow{v}$ of the shell is arbitrary in real situations, $\widehat{i}$ is not matched to $\widehat{s}_v$ or $\widehat{s}_h$. Thus, the RCS of a flying shell is usually different from RCS_{VV} or RCS_{HH}, which are stored in the RCS database.

In practice, the received RCS by an antenna system whose copolarization direction is $\widehat{i}$ RCS_r can be represented by a linear combination of RCS_{VV}, RCS_{HH}, RCS_{VH}, and RCS_{HV} as follows:

$$\begin{aligned} RCS_r &= \cos\theta_1 RCS_{VV} + \cos\theta_2 RCS_{HH} \\ &\quad + \cos\theta_1 RCS_{VH} + \cos\theta_2 RCS_{HV} \\ &\approx \cos\theta_1 RCS_{VV} + \cos\theta_2 RCS_{HH} \end{aligned} \tag{2}$$

where

$$\cos\theta_1 = \widehat{i} \cdot \widehat{s}_v$$
$$\cos\theta_2 = \widehat{i} \cdot \widehat{s}_h$$
$$\widehat{s}_v = \frac{\widehat{r} \times \widehat{s}_h}{|\widehat{r} \times \widehat{s}_h|} = x'\cos\theta\cos\phi + y'\cos\theta\sin\phi - \widehat{z}'\sin\theta$$
$$\widehat{s}_h = \frac{\widehat{r} \times \widehat{z}'}{|\widehat{r} \times \widehat{z}'|} = -x'\sin\phi + y'\cos\phi$$

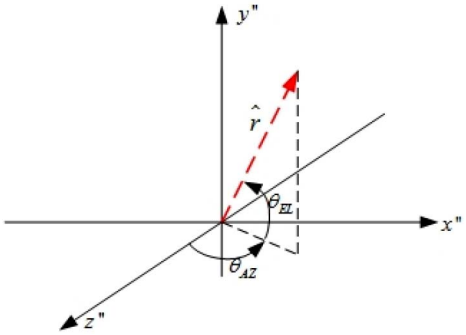

Fig. 5. Radar coordinate system.

where θ_1 is the angle between $\widehat{s}_v$ and $\widehat{i}$, θ_2 is the angle between $\widehat{s}_h$ and $\widehat{i}$, and $\times$ denotes the cross product. Moreover, RCS_{VH} and RCS_{HV} are cross-polarized RCSs with vertical-to-horizontal (VH) and horizontal-to-vertical (HV) polarizations, respectively. In (2), we assumed that the copolarized RCS_{VV} and RCS_{HH} are much larger than the cross-polarized RCS_{VH} and RCS_{HV}.

Next, it should be noted that the RLOS unit vector $\widehat{r}$ changes at every PRI because the radar tracks the shell during a tracking interval. Thus, $\widehat{i}$ is also a function of time. A radar coordinate system to find $\widehat{i}$ is illustrated in Fig. 5.

In Fig. 5, y'' denotes the initial direction of antenna copolarization, and z'' denotes the initial direction of the antenna beam. Let y'' and $\widehat{z}''$ be the unit vectors along y'' and z'', respectively. Then, ω, u, and v are defined as follows:

$$\begin{aligned} \omega &= \cos\theta_{EL}\cos\theta_{AZ} \\ u &= \cos\theta_{EL}\sin\theta_{AZ} \\ v &= \sin\theta_{EL} \end{aligned} \tag{3}$$

where

$$\begin{aligned} \theta_{EL} &= 90 - \cos^{-1}\left(\widehat{r}\cdot y''\right) \\ \theta_{AZ} &= \tan^{-1}\left(\frac{\widehat{r}\cdot\left(y''\times\widehat{z}''\right)}{\widehat{r}\cdot\widehat{z}''}\right). \end{aligned}$$

Finally, $\widehat{i}$ can be found using Ludwig definition III [13] as follows:

$$\widehat{i} = -x''\left(\frac{uv}{1+\omega}\right) + y''\left(1-\frac{v^2}{1+\omega}\right) - \widehat{z}''v. \tag{4}$$

Consequently, the RCS of a flying shell RCS_r can be obtained using (2) and (4).

III. Design of Fuzzy Classifier

A. MF in Fuzzy Set Theory

Unlike a conventional set, a fuzzy set expresses the degree to which an element belongs to a set [14]. If X is a collection of elements denoted generically by x, then fuzzy set A in X is defined as a set of ordered pairs

$$A = \{(x, F_A(x)) \,|x \in X\} \tag{5}$$

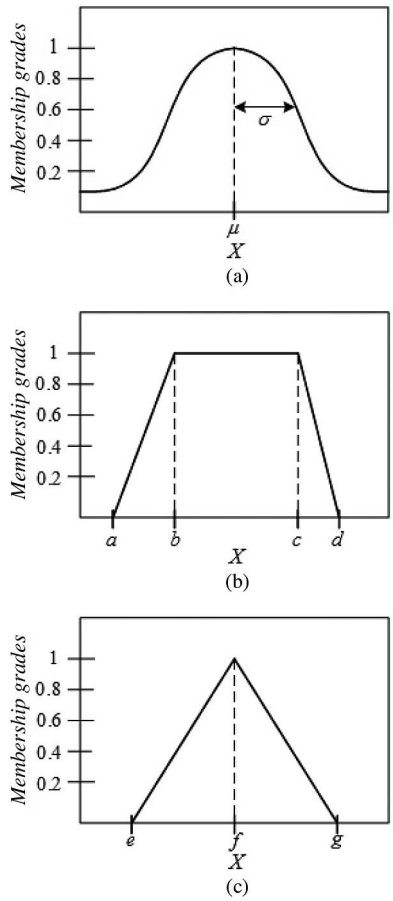

Fig. 6. Three different types of MFs. (a) Gaussian MF. (b) Trapezoidal MF. (c) Triangular MF.

where $F_A(x)$ denotes the MF for the fuzzy set A. The MF maps each element x of X to a membership grade (MG) between 0 and 1. Among various types of MFs, we use three different MFs (Gaussian, trapezoidal, and triangle MFs), as shown in Fig. 6.

In Fig. 6(a), μ denotes the centre of the Gaussian MF, and σ is the parameter which determines the width of the Gaussian MF. In addition, the parameters $\{a, b, c, d\}$ (with $a < b < c < d$) and $\{e, f, g\}$ (with $e < f < g$) in Fig. 6(b) and (c) determine the x coordinates of the four corners of the trapezoidal MF and the three corners of the triangular MF, respectively.

We are able to design the three different fuzzy classifiers using the three types of MFs, respectively. If the Gaussian fuzzy classifier is utilized to classify the shells of L target classes, the fuzzy classifier consists of L Gaussian MFs. The classification scheme using each fuzzy classifier is very simple. It should be noted that the performance of the fuzzy classifier using each specific MF depends only on the selection of given parameters of the MF, which are usually unknown. In this paper, after the Firefinder starts to track a flying shell, the input value of the fuzzy classifier $\overline{RCS_r}$ is computed by averaging RCS_r during tracking time as follows:

$$\overline{RCS_r} = \frac{1}{P}\sum_{m=1}^{P} RCS_r(m) \tag{6}$$

where $RCS_r(m)$ denotes the received RCS at the mth observation, and P denotes the total number of observations during the measurement time.

When $\overline{RCS_r}$ is used as an input to the fuzzy classifier, we can easily find the MGs that the $\overline{RCS_r}$ belongs to in each target class. Then, the true target class i^* can be determined by the class of MF having the maximum MG

$$i^* = \max_k F_k\left(\overline{RCS_r}\right), \quad k = 1, \ldots, L \tag{7}$$

where $F_k\left(\overline{RCS_r}\right)$ denotes the MF which maps the given $\overline{RCS_r}$ to a specific MG corresponding to the kth target class, and L denotes the number of target classes to be classified.

B. Determination of MF Parameters

The fuzzy classifier can complete the classification task within a very short time. This is because the classification requires L simple evaluations of MGs [i.e., simple mappings $\overline{RCS_r}$ to $F_k\left(\overline{RCS_r}\right)$] and only one comparison of the MGs (i.e., finding the maximum value). Thus, it is the most appropriate for the Firefinder radar that has a time-critical mission. As stated, the performance of the fuzzy classifier is very sensitive to how we choose the parameters of MFs. In other words, the wrong selection of parameters can degrade the classification accuracy of the fuzzy classifier. Thus, the parameters which control the locations and the detailed shapes of the MFs (i.e., $\mu, \sigma, a, b, c, d, e, f$, and g in Fig. 6) should be optimized to maximize the classification capability. To achieve this goal, a simple exhaustive search method which checks all possible candidates of unknown parameters can be used. However, choosing the optimal parameters using this method in multidimensional space requires a very long computation time. Thus, the random search method, which effectively finds the global optimum by a specific rule, can be considered as an alternative. Among a variety of random search methods, we selected the PSO algorithm.

The PSO algorithm is a stochastic search method that has been shown to be effective in optimizing difficult multidimensional discontinuous problems in a variety of fields [15], [16]. In the PSO algorithm, particles move through the search space using a combination of an attraction to the best solution that they individually have found, and an attraction to the best solution that any particle in their *neighborhood* has found [17]. The detailed procedure of the PSO algorithm is described in [15]–[17].

In this paper, each particle consists of the parameters of the MFs. For example, if we select a Gaussian fuzzy classifier where the number of parameters is two (i.e., μ and σ) and the number of target classes is L, each particle consists of 2 L-dimensional vectors. Then, the particles are moved to maximize the classification accuracy using the training database.

In order to optimize the fuzzy classifier, the cost function is defined as follows:

$$P_c = \frac{N_c}{N_t} \tag{8}$$

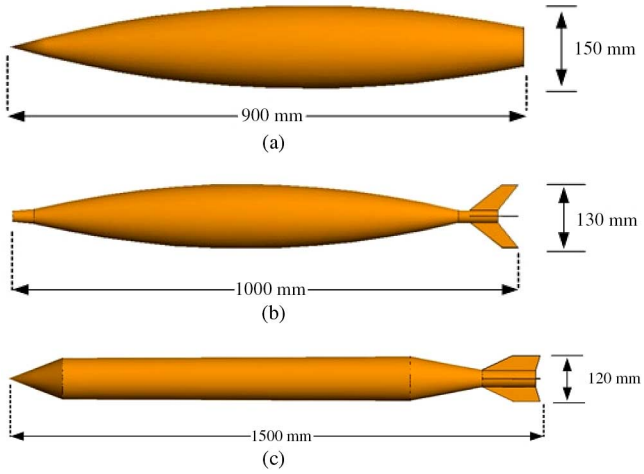

Fig. 7. Three shell-shaped targets. (a) Target 1. (b) Target 2. (c) Target 3.

where N_t denotes the total number of classifications, N_c denotes the number of correct classifications, and P_c denotes the classification accuracy.

IV. Numerical Results

To demonstrate the classification capability of the fuzzy classifier designed by the proposed scheme, we conducted classification experiments using three different shell-shaped targets, as shown in Fig. 7 (i.e., the number of targets L is 3).

The construction of the RCS database was carried out using the commercial software FEKO at a frequency of 5 GHz. In Fig. 8, it is noted that the bodies of three targets are geometrically symmetric along both the azimuth and elevation axes. Thus, the azimuth angle ϕ was varied from 0° to 180° with a 1° step (i.e., M is 181 samples for each target), and the elevation angle θ was varied from 0° to 90° with a 1° step (i.e., N is 91 samples for each target). Furthermore, because two polarizations such as VV and HH are used for the construction of the RCS database, the total number of RCS values in the RCS database is $2 \times L \times M \times N = 98\,826$. The RCS database for classification is shown in Fig. 8.

In order to create the training database, flight scenarios of the three different shell-shaped targets were varied depending on four variables: the initial azimuth angle of fire ϕ', initial elevation angle of fire θ', initial speed of shells v_{In}, and distance from the fire to the Firefinder radar y_d, as shown in Fig. 9.

In Fig. 9, we assumed that the shell is fired at the origin and the Firefinder radar is located at y_d on the y axis. After firing, the trajectory of shell is assumed to be affected only by gravity. The detailed parameters of flight scenarios used to generate the training database for each target are summarized in Table I.

According to Table I, the number of flight scenarios for each target is 13 (the number of ϕ') $\times$ 4 (the number of θ') $\times$3 (the number of v_{In}) $\times$5 (the number of y_d) $= 780$, and the total number of the entire training database is 780×3 (the number of targets) = 2340. In the predefined flight scenarios, Firefinder starts to track shells starting from θ_{EL}, which is an angle randomly selected between 0° and 1°, and continuously collects RCS during tracking interval T, as shown in Fig. 10. In this

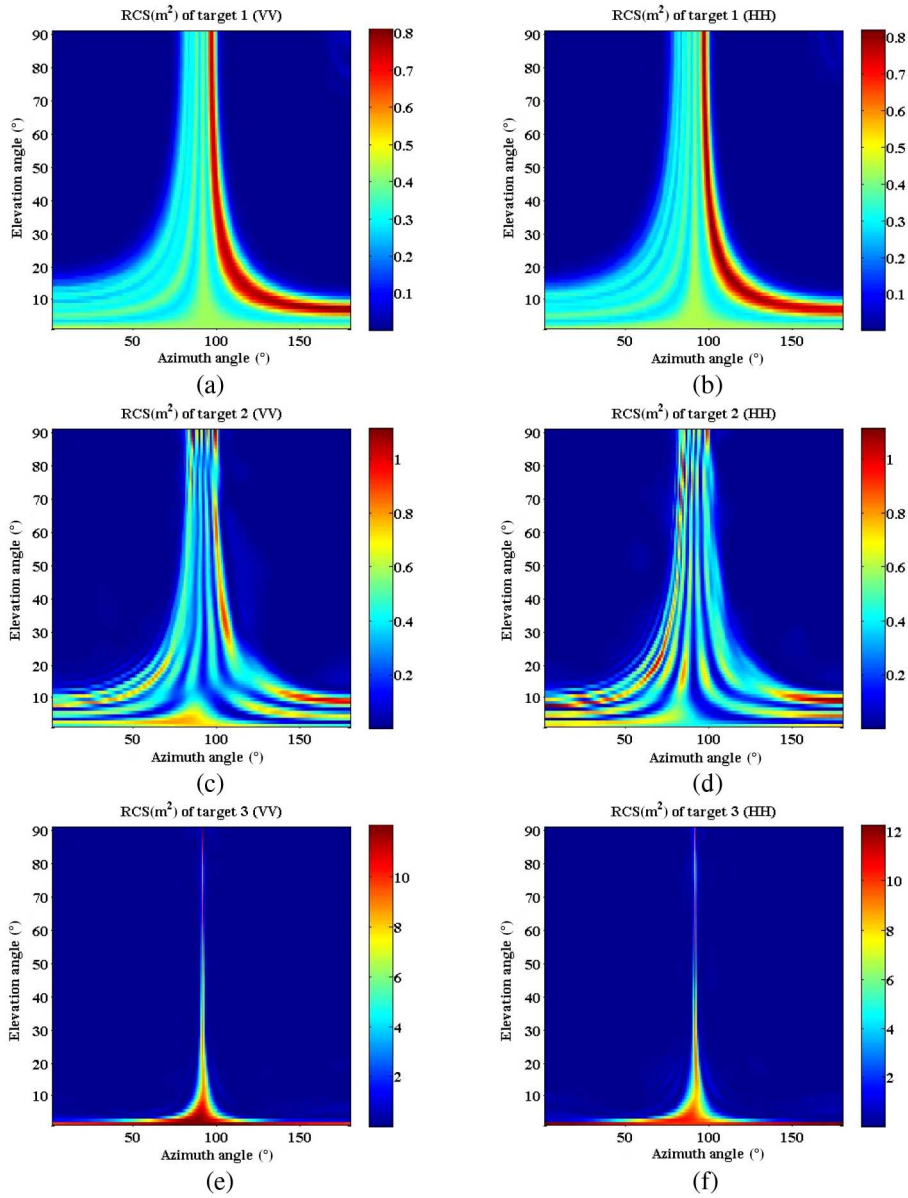

Fig. 8. RCS database related to each target. (a) Target 1 (VV). (b) Target 1 (HH). (c) Target 2 (VV). (d) Target 2 (HH). (e) Target 3 (VV). (f) Target 3 (HH).

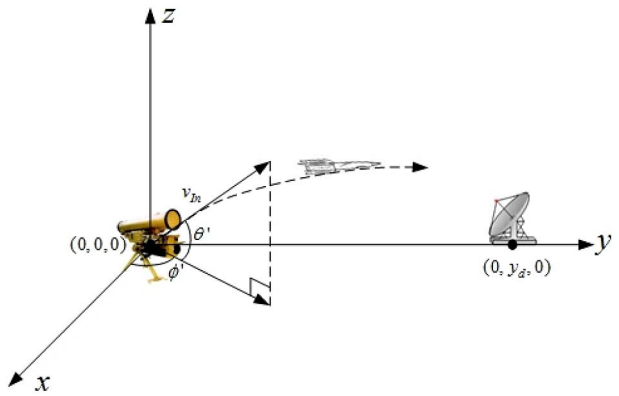

Fig. 9. Flight scenarios of shell.

paper, T was chosen as 1 s, and the PRF of the Firefinder radar was 1 kHz.

As mentioned in Section II-D, many RCS_rs during T [e.g., $1\ (\mathrm{s}) \times 1000\ (\mathrm{Hz}) = 1000$ in this paper] for each flight scenario were obtained using (2) and (4). In this paper, y'' and z'' were assumed to be [0, 0, 1] and [-1, 0, 0], respectively. Next, $\overline{RCS_r}$s for each scenario were computed by averaging collected RCS_rs using (6) with $P = 1000$. Then, the entire training database consists of the computed 2340 $\overline{RCS_r}$s from 2340 different scenarios.

Before we optimized the parameters of MFs with PSO, we accomplished the initialization of MFs using the given training database. Because the number of targets L is three, we have three MFs to be initialized. Based on Table I, the entire training database consists of three subtraining databases such as $\overline{RCS_{r1}}$, $\overline{RCS_{r2}}$, and $\overline{RCS_{r3}}$, which correspond to Targets 1–3, as follows:

TABLE I
PARAMETERS OF FLIGHT SCENARIOS CORRESPONDING TO THREE DIFFERENT TARGETS

Target class	Parameter	Range	Step
Target 1	ϕ' (°)	30–150	10
	θ' (°)	25–40	5
	v_{In} (m/s)	200–400	100
	y_d (km)	10–50	10
Target 2	ϕ' (deg)	30–150	10
	θ' (deg)	30–45	5
	v_{In} (m/s)	100–300	100
	y_d (km)	5–45	10
Target 3	ϕ' (deg)	30–150	10
	θ' (deg)	20–35	5
	v_{In} (m/s)	400–600	100
	y_d (km)	40–80	10

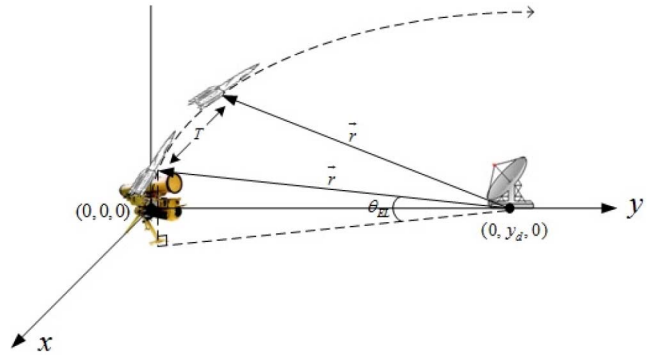

Fig. 10. Observation angle during tracking.

$$\overline{RCS_{train}} = \bigcup \overline{RCS_{rk}}, \quad k = 1, 2, 3 \tag{9}$$

where $\overline{RCS_{train}}$ denotes the entire training database, $\overline{RCS_{rk}}$ denotes the subtraining database related to the kth target, and $\bigcup(\cdot)$ is the union set.

Then, the parameters of the MF related to the kth target were initialized using $\overline{RCS_{rk}}$. Let $\widehat{\mu}\left(\overline{RCS_{rk}}\right)$ and $\widehat{\sigma}\left(\overline{RCS_{rk}}\right)$ be the mean and the standard deviation of $\overline{RCS_{rk}}$, respectively. Then, the initial parameters of MF are determined depending on the types of MF. In the case of the Gaussian MF, μ is chosen as $\widehat{\mu}\left(\overline{RCS_{rk}}\right)$ and σ as $\widehat{\sigma}\left(\overline{RCS_{rk}}\right)$. In the case of the trapezoidal MF, a and d are located at a distance of $\widehat{\sigma}\left(\overline{RCS_{rk}}\right)$ from $\widehat{\mu}\left(\overline{RCS_{rk}}\right)$. In addition, b and c are located at a distance of $\widehat{\sigma}\left(\overline{RCS_{rk}}\right)/2$ from $\widehat{\mu}\left(\overline{RCS_{rk}}\right)$. In the case of a triangular MF, f is chosen as $\widehat{\mu}\left(\overline{RCS_{rk}}\right)$. Furthermore, e and g are $\widehat{\sigma}\left(\overline{RCS_{rk}}\right)$ away from $\widehat{\mu}\left(\overline{RCS_{rk}}\right)$.

After we initialize the MFs, some parameters (i.e., a, b, and e) of the MFs can be positioned on the negative $\overline{RCS_r}$ axis because of the statistical distribution of $\overline{RCS_{rk}}$ (e.g., $\widehat{\mu}\left(\overline{RCS_{rk}}\right) - \widehat{\sigma}\left(\overline{RCS_{rk}}\right) < 0$). In this case, the negative parts of the MFs do not participate in the classification task because $\overline{RCS_r}$ should be positive. Thus, the additional shifts of MF parameters are further applied as follows:

$$MF_P = \begin{cases} MF_P, & MF_P > 0 \\ 0, & MF_P < 0 \end{cases} \tag{10}$$

where MF_P denotes the locations of MF parameters (i.e., a, b, and e) on the $\overline{RCS_r}$ axis. The initialized MFs in the three different fuzzy classifiers are shown in Fig. 11. In Fig 11, the horizontal axis denotes $\overline{RCS_r}$, and the vertical axis denotes the MG. In Fig. 11, it is noted that $\overline{RCS_r}$ of the three targets obtained from various flight scenarios are concentrated between 0 and $0.06\ \mathrm{m}^2$, while the entire RCS database in Fig. 8 has large RCS values up to $12\ \mathrm{m}^2$. Thus, it is recommended that, when optimizing MF parameters, using the training database based on flight scenarios is more efficient than using the entire RCS database, as mentioned in Section II-B.

Next, the initial parameters in Fig. 11 were further optimized using PSO. The number of maximum iterations t was fixed at 30, and the number of particles was set to 100. Each initial particle was generated by adding a value selected randomly between 0 and the maximum RCS in the training database. In addition, the initial velocity of each particle was chosen randomly between -1 and 1.

In the PSO algorithm, additional shifts using (10) were also applied to MF parameters (i.e., μ, a, b, c, d, e, f, and g) at each iteration such that MFs should not go into the negative $\overline{RCS_r}$ region owing to random movements of the particles. Let x_{gbest} denote the best parameters found by swarm at each iteration. Then, Fig. 12 presents $P_{c,gbest}$ (i.e., P_c at x_{gbest}) versus the iteration number. In Fig. 12, the initial $P_{c,gbest}$ of the Gaussian fuzzy classifier is more accurate than those of other fuzzy classifiers. This is because the Gaussian distribution is more suitable for describing the statistical distribution of the training database. In addition, $P_{c,gbest}$ of the Gaussian fuzzy classifier remains fixed at 72% even though the iteration increases. The trapezoidal fuzzy classifier shows a very low initial $P_{c,gbest}$ because a major portion of three MFs corresponding to three different shells overlap each other, as shown in Fig. 11(b). Nevertheless, as seen in Fig. 12(b), $P_{c,gbest}$ improves rapidly as iteration number t increases. Consequently, $P_{c,gbest}$ at $t = 30$ approaches approximately 70%. In the case of a triangular fuzzy classifier, the initial $P_{c,gbest}$ is approximately 50%, but $P_{c,gbest}$ exceeds 70% at $t = 30$. The final MFs of each fuzzy classifier at x_{gbest} after 30 iterations are shown in Fig. 13. In addition, the optimized final MF parameters are summarized in Table II.

It should be noted that θ', v_{In}, and y_d of the shells typically have very limited ranges depending on the type of shell. However, ϕ' can be varied widely from 0° to 360° in real situations, regardless of the types of the shells. Thus, although we optimize the MF parameters according to Table I in the training phase, ϕ' in real situations can significantly deviate from the range of ϕ' used for the training database.

In order to compare the performances of the designed three fuzzy classifiers, two different test sets, SET-1 and SET-2, were formed. In SET-1, each test flight scenario is determined by the four variables ϕ', θ', v_{In}, and y_d, which were selected randomly in the ranges of the variables in Table I. Then, $100\,(\text{number of test scenarios for each target}) \times 3\,(\text{number of targets})$ 300 test flight scenarios were generated

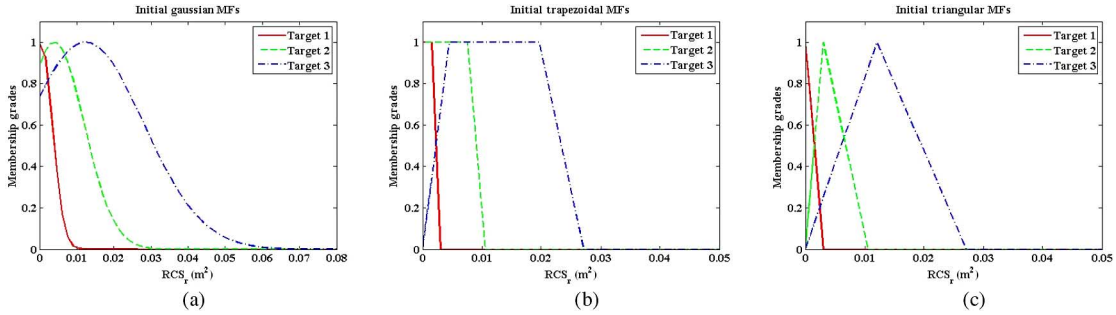

Fig. 11. Initial MFs in each fuzzy classifier. (a) Gaussian MFs. (b) Trapezoidal MFs. (c) Triangular MFs.

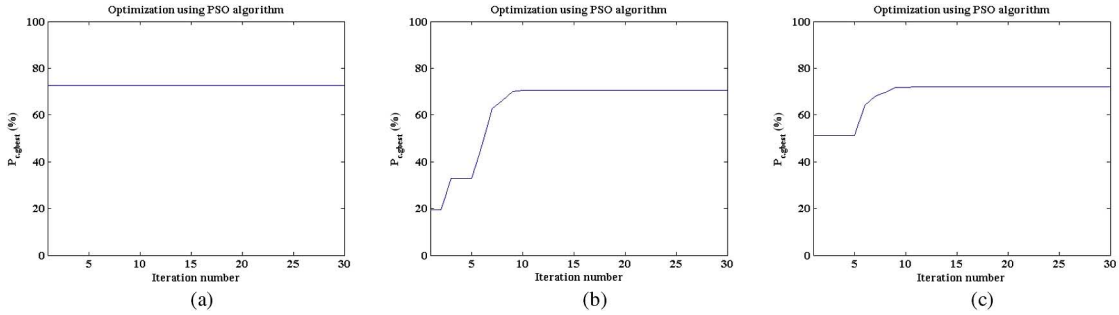

Fig. 12. $P_{c,gbest}$ versus iteration number. (a) Gaussian MFs. (b) Trapezoidal MFs. (c) Triangular MFs.

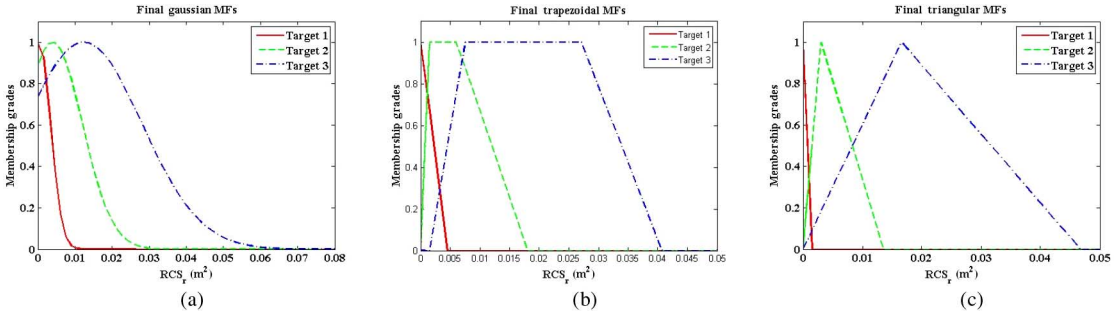

Fig. 13. Final MFs in each fuzzy classifier. (a) Gaussian MFs. (b) Trapezoidal MFs. (c) Triangular MFs.

TABLE II
FINAL PARAMETERS OF THREE DIFFERENT FUZZY CLASSIFIERS

Fuzzy classifier	Target class	Parameter			
		μ	σ		
Gaussian	Target 1	0.00035	0.003		
	Target 2	0.0039	0.008		
	Target 3	0.0123	0.0157		
		a	b	c	d
Trapezoidal	Target 1	0	0	0	0.0045
	Target 2	0	0.0015	0.006	0.0181
	Target 3	0.0015	0.0075	0.0302	0.0452
		e	f	g	
Triangular	Target 1	0	0	0.0015	
	Target 2	0	0.003	0.0136	
	Target 3	0	0.0166	0.0467	

for SET-1, yielding 300 $\overline{RCS_r}$s obtained by using the same process as in the training phase.

In SET-2, the three variables θ', v_{In}, and y_d of each test flight scenario were chosen randomly within the ranges of the variables in Table I, whereas ϕ' of each test scenario was chosen randomly between 0° and 180° to consider more realistic situations. Then, 300 $\overline{RCS_r}$s corresponding to $100\,(\text{number of test scenarios for each target}) \times 3\,(\text{number of targets})$ 300 test flight scenarios were obtained by using the same process as in the training phase. It is noted that the range of ϕ' for SET-2 is different from that used for training phase (i.e., Table I). Thus, it is expected that classification capability of the fuzzy classifier for SET-2 will be inferior to that for SET-1.

The classification capabilities of three fuzzy classifiers were analyzed against the signal-to-noise ratio (SNR). Thus, the additive white Gaussian noises (AWGNs) were added to RCS_rs obtained in the testing phase to achieve the desired SNR level, which varied from 0 to 30 dB with a 5 dB step.

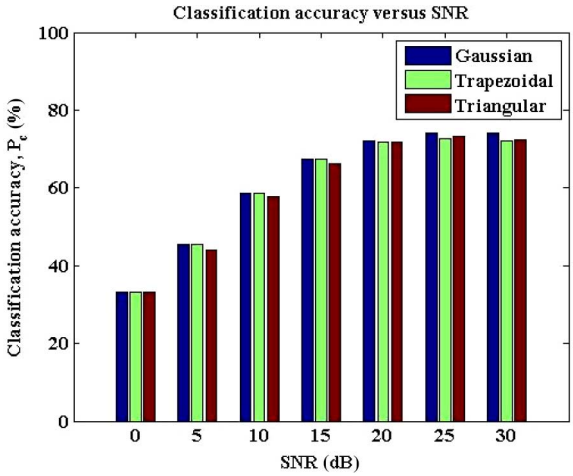

Fig. 14. P_c of three fuzzy classifiers versus SNR for the SET-1.

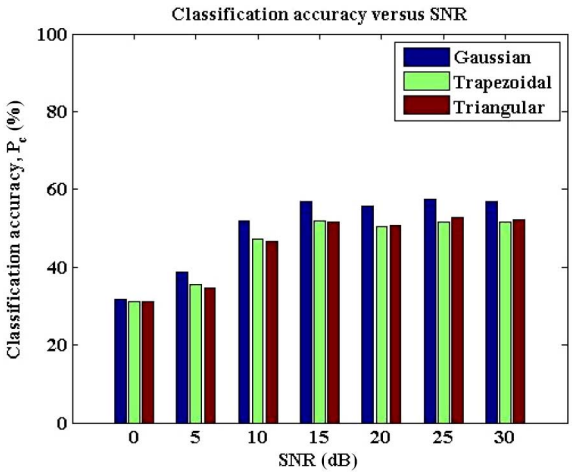

Fig. 15. P_c of three fuzzy classifiers versus SNR for the SET-2.

Figs. 14 and 15 show the values of P_c for the three designed fuzzy classifiers versus the SNR for SET-1 and SET-2, respectively. In Fig. 14, the Gaussian classifier exhibits a slightly better P_c than other classifiers over the entire range of SNR levels. The classification accuracies of the three designed fuzzy classifiers improve as the SNR level increases.

In Fig. 15, the performances of the three fuzzy classifiers for SET-2 degrade compared with those for SET-1. As mentioned above, this is because the range of ϕ' for SET-2 (i.e., $\phi' : 0^\circ - 180^\circ$) contains angles which were not covered in the training phase (i.e., $\phi' : 0^\circ - 30^\circ,\ 150^\circ - 180^\circ$), while the range of ϕ' for SET-1 is identical to that for the training phase. Among the three fuzzy classifiers, the Gaussian fuzzy classifier exhibits the best classification performance. This means that the Gaussian MF is more appropriate for the Firefinder radar than for other MFs in real situations.

V. Conclusion

In this paper, we presented a detailed procedure for designing fuzzy classifiers to classify shell-shaped targets. Because the Firefinder radar requires a time-critical mission, only the RCS of the shells (rather than HRRP, ISAR, or micro-Doppler signature) was used for classification. To construct the training database, the RCSs of shells considering the relative orientation angle and polarization dependences were obtained in various flight scenarios based on real situations. Then, MFs of the Gaussian, trapezoidal, and triangular fuzzy classifiers were optimized using PSO to find optimal parameters of the MFs. In addition, classification experiments using two different test datasets were conducted to evaluate the performances of the three fuzzy classifiers. Results show that the proposed scheme can provide three fuzzy classifiers that can classify shells using only RCS. In addition, the Gaussian fuzzy classifiers are more suitable for Firefinder radar than the trapezoidal and triangular fuzzy classifiers.

It should be noted that various fuzzy classifiers using different features such as drag coefficients, muzzle velocity of shells, elevation angle of fire, and RCS can be designed to classify shell targets. Furthermore, the fusion of multiple fuzzy classifiers can be easily accomplished by using simple inference procedures of fuzzy reasoning. Thus, it is expected that the performance of the fuzzy classifier can be significantly improved by combining the multiple fuzzy classifiers using multiple features such as RCS, drag coefficients, muzzle velocity of shells, and elevation angle of fire, compared with the fuzzy classifier using only RCS.

Acknowledgment

The authors would like to thank the associated editor and the anonymous reviewers for their valuable comments and suggestions to improve the quality of this paper.

References

[1] E.-P. Lam, H.-W. Birrell, and J. Magallon, "System performance prediction of Firefinder radar," in *Proc. IEEE Syst. Conf.*, Apr. 2010, pp. 500–504.

[2] D.-Q. Zhou, "Study of key techniques applied in radars of locating enemy artilleres," in *Proc. IEEE Int. Conf. Microw. Millimeter Wave Technol. (ICMMT)*, Apr. 2007, pp. 1–4.

[3] E.-P. Lam, H.-W. Birrell, and J. Magallon, "Performance prediction of Firefinder radar using high fidelity simulation," in *Proc. IEEE Radar Conf.*, May 2010, pp. 48–53.

[4] J. Gu, M. Shi, and S. Fan, "An impact point of shipboard artillery shell calculating system based on DSP and matlab-simulink simulation," in *Proc. IEEE Int. Conf. Comput. Des. Appl. (ICCDA)*, Jun. 2010, vol. 3, pp. 565–567.

[5] M.-A. Zaman and M.-A. Matin, "Radar cross section calculation of a shell-shaped projectile using Bezier curves and physical optics," in *Proc. IEEE 7th Int. Conf. Electr. Comput. Eng. (ICECE)*, Dec. 2012, pp. 690–693.

[6] D. John, F. Christopher, and M. Lee, "FIREFINDER: Position analysis system advanced development model," *IEEE Trans. Aerosp. Electron. Syst. Mag.*, vol. 11, no. 9, pp. 25–29, Sep. 1996.

[7] W. Fisherbein, "Firefinder, a radar forty years in the making," *IEEE Trans. Aerosp. Electron. Syst.*, vol. 44, no. 2, pp. 817–829, Apr. 2008.

[8] K.-T. Kim, D.-K. Seo, and H.-T. Kim, "Efficient radar target recognition using the MUSIC algorithm and invariant features," *IEEE Trans. Antennas Propag.*, vol. 50, no. 3, pp. 325–337, Mar. 2002.

[9] K.-T. Kim, D.-K. Seo, and H.-T. Kim, "Efficient classification of ISAR images," *IEEE Trans. Antennas Propag.*, vol. 53, no. 5, pp. 1611–1621, May 2005.

[10] S.-C. Chan and K.-C. Lee, "Radar target recognition by MSD algorithms on angular-diversity RCS," *IEEE Antennas Wireless Propag. Lett.*, vol. 12, pp. 937–940, Jul. 2013.

[11] A. Register, W. D. Blair, L. Ehrman, and P. K. Willett, "Using measured RCS in a serial, decentralized fusion approach to radar-target classification," in *Proc. IEEE Aerosp. Conf.*, Mar. 2008, pp. 1–8.
[12] W. C. Gibson, *The Method of Moments in Electromagnetics*. London, U.K.: Chapman & Hall, 2007.
[13] A. C. Ludwig, "Definition of cross polarization," *IEEE Trans. Antennas Propag.*, vol. 21, no. 1, pp. 116–119, Jan. 1973.
[14] J.-S. R. Jang, C.-T. Sun, and E. Mizutani, *Neuro-Fuzzy and Soft Computing*. Englewood Cliffs, NJ, USA: Prentice-Hall, 1996.
[15] J. Robinson and Y. Rahmat-Samii, "Particle swarm optimization in electromagnetics," *IEEE Trans. Antennas Propag.*, vol. 52, no. 2, pp. 397–407, Feb. 2004.
[16] S.-H. Park and H.-T. Kim, "Stepped-frequency ISAR motion compensation using particle swarm optimization with an island model," *Prog. Electromagn. Res.*, vol. 85, pp. 25–37, 2008.
[17] D. Bratton and J. Kennedy, "Defining a standard for particle swarm optimization," in *Proc. IEEE Swarm Intell. Symp. (SIS)*, Apr. 2007, pp. 120–127.

Seung-Jae Lee received the B.S. degree in electronics and communication engineering from Hanyang University, Ansan, Korea, in 2012, and the M.S. degree in electrical engineering from Pohang University of Science and Technology (POSTECH), Pohang, Korea, in 2014. He is currently pursuing the Ph.D. degree in radar and electromagnetics signal processing at POSTECH.

His research interests include radar signal processing, radar imaging, radar target recognition, and pattern recognition.

Seong-Jae Jeong received the B.S. and M.S. degrees in electronic engineering from Dongguk University, Seoul, Korea, in 2010 and 2012, respectively. He is currently pursuing the Ph.D. degree in electrical engineering from Pohang University of Science and Technology (POSTECH), Pohang, Korea.

From 2013 to 2014, he was a Research Member with the Department of Electrical Engineering, POSTECH. His research interests include radar target imaging and recognition, and polarimetric radar imaging and recognition.

Byung-Soo Kang received the B.S. degree in electronic engineering from Yeungnam University, Gyeongsan, Korea, in 2012, and the M.S. degree in electrical engineering from Pohang University of Science and Technology (POSTECH), Pohang, Korea, in 2014. He is currently pursuing the Ph.D. degree in radar and electromagnetics signal processing at POSTECH.

His research interests include radar signal processing, automotive radar signal processing, inverse synthetic aperture radar (ISAR) imaging, and target motion compensation.

Hyun Kim received the B.S., M.S., and Ph. D. degrees in electrical and electronics engineering from Yonsei University, Seoul, Korea, in 2002, 2005, and 2011, respectively.

He is currently a Research Engineer with LIG Nex1, Yongin, Korea. His research interests include numerical analysis, phased array antenna, and radar systems.

Sang-Mi Chon received the B.S. and Ph.D. degrees in electrical engineering from Pohang University of Science and Technology (POSTECH), Pohang, Korea, in 1999 and 2006, respectively.

After graduation, she joined LIG NEX1, Yongin, Korea. Her research interests include antennas and radars.

Hyung-Gi Na received the B.S., M.S., and Ph.D. degrees in electrical engineering from Pohang University of Science and Technology (POSTECH), Pohang, Korea, in 1991, 1993, and 1996, respectively.

After graduation, he joined LIGNEX1, Yongin, Korea. His research interests include antennas and radars.

Kyung-Tae Kim received the B.S., M.S., and Ph.D. degrees in electrical engineering from Pohang University of Science and Technology (POSTECH), Pohang, Korea, in 1994, 1996, and 1999, respectively.

From 2002 to 2010, he was a Faculty Member with the Department of Electronic Engineering, Yeungnam University, Gyeongsan, Korea. He is currently an Associate Professor with the Department of Electrical Engineering, POSTECH. He is the Director of the Sensor Target Recognition Laboratory, sponsored by the Defense Acquisition Program Administration (DAPA) and the Agency for Defense Development (ADD), and the Radar and ElectroMagnetics Signal Processing (REMS) Laboratory, POSTECH. His research interests include radar signal processing with a special emphasis on multi-input multi-output radar, SAR and ISAR imaging, and NCTR and ATR.